Dual-functional Cellular and Radar Transmission: Beyond Coexistence

(Invited Paper)

Fan Liu*†, Longfei Zhou‡, Christos Masouros†, Ang Li†, Wu Luo‡ and Athina Petropulu§
*School of Information and Electronics, Beijing Institute of Technology, Beijing, China
†Department of Electronic and Electrical Engineering, University College London, London, UK
‡State Key Laboratory of Advanced Optical Communication Systems and Networks, Peking University, Beijing, China
§Department of Electrical and Computer Engineering, Rutgers, The State University of New Jersey, NJ 08854, USA
Email: liufan92@bit.edu.cn, {zhoulongfei, luow}@pku.edu.cn, {c.masouros, ang.li.14}@ucl.ac.uk, athinap@rutgers.edu

***Abstract*—We propose waveform design for a dual-functional multi-input-multi-output (MIMO) system, which carries out both radar target detection and multi-user communications using a single hardware platform. By enforcing both a constant modulus (CM) constraint and a similarity constraint with respect to referenced radar signals, we aim to minimize the downlink multi-user interference. Unlike conventional approaches which obtain suboptimal solutions to the generally NP-hard CM optimization problems involved, we propose a branch-and-bound method to efficiently find the global minimizer of the problem. Simulations show that the proposed algorithm significantly outperforms the state-of-art by achieving a favorable trade-off between radar and communication performance.**

I. Introduction

The limited bandwidth is the bottleneck in the development of future wireless technologies. As the number or communication devices and services increases, there is need for more spectrum. On the other hand, the spectrum earmarked for radar applications is under-utilized. In view of this, the spectrum regulators are now seeking the possibility for releasing spectral bands previously available to radars only, for shared used by radar and communication systems [1]. This has motivated work on spectrum sharing that controls the interference between radar and communication systems. Recent works on coexistence of MIMO radar and communication systems can be found in [2]–[4].

In a cooperative coexistence scenario, the signaling schemes of the cooperating systems are designed by an entity that plays the role of a moderator [2]. The systems are required to share with the moderator node information such as channel state information (CSI), or radar probing waveforms, which might not be always easy to implement in practice. Given both the computational and hardware costs of the coexistence schemes, a more favorable approach is to design a dual-functional waveform, referred as the RadCom waveform, which realizes both radar and multi-user communication operations on a single platform. In such designs, the information bits are typically modulated by varying the sidelobe levels of radar beampatterns [5], or by shuffling the radar transmit waveforms across the antennas [6]. In these approaches, each communication symbol is represented by one or more radar pulses, which results in a low data rate of the order of the pulse repetition frequency (PRF) of radar. To address this issue, the work of [7] develops a series of beamforming approaches to support simultaneous target detection and multi-user communications, which will not affect the original modulation scheme and the data rate of the communication system. However, the beamforming approaches in [7] only focus on the average power constraints, and do not address the design of constant modulus (CM) signals.

In practice, for both radar and communications, the utilization of constant modulus waveforms can avoid signal distortion when low-cost non-linear power amplifiers are used. Design of such waveforms has been addressed for MIMO radar and massive MIMO communication systems via various optimization techniques, such as Semidefinite Relaxation (SDR) [8], manifold based algorithm [9] and successive Quadratic Constrained Quadractic Programming (QCQP) Refinement (SQR) [10]. However, due to the non-convexity and NP-hardness underlying the CM constrained problems, only suboptimal solutions can be obtained by the aforementioned methods. To the best of our knowledge, efficient *global algorithms* for CM waveform design have received little attention in the existing literature.

This paper considers a CM waveform design for dual-functional MIMO RadCom systems, where the downlink multi-user interference (MUI) is minimized under both constant modulus and radar signal similarity constraints. In contrast to existing approaches that only guarantee the local optimality of the solutions, our technique can efficiently yield the *global minimizer* of the problem by using a branch-and-bound (BnB) algorithm. Numerical results show that the proposed algorithm considerably outperforms the conventional SQR algorithm in terms of the performance trade-off between communications and radar.

II. Problem Formulation

We consider a dual-functional MIMO RadCom system, which simultaneously transmits radar probing waveforms and communication symbols to downlink users. The joint system is equipped with a uniform linear array (ULA) with N antennas, serving K single-antenna users, while looking for radar targets

at the same time. The received symbol matrix at the downlink users can be given as

$$\mathbf{Y} = \mathbf{HX} + \mathbf{W}, \tag{1}$$

where $\mathbf{X} = [\mathbf{x}_1, \mathbf{x}_2, ..., \mathbf{x}_L] \in \mathbb{C}^{N\times L}$ is the transmitted signal matrix, with L being the length of the communication frame, $\mathbf{H} = [\mathbf{h}_1, \mathbf{h}_2, ..., \mathbf{h}_K]^T \in \mathbb{C}^{K\times N}$ is the channel matrix, and $\mathbf{W} = [\mathbf{w}_1, \mathbf{w}_2, ..., \mathbf{w}_L] \in \mathbb{C}^{K\times L}$ is the noise matrix, with $\mathbf{w}_j \sim \mathcal{CN}(0, N_0\mathbf{I}_N), j = 1, 2, ..., L$.

Following [7], we rely on the following assumptions: 1) The transmitted signal matrix $\mathbf{X}$ is used as dual-functional waveform for both radar and communication operations; 2) The downlink channel $\mathbf{H}$ is flat Rayleigh fading, and remains unchanged during one communication frame/radar pulse; 3) The channel $\mathbf{H}$ is perfectly estimated by pilot symbols.

Given the desired constellation symbol matrix $\mathbf{S} \in \mathbb{C}^{K\times L}$ for downlink users, the received signals can be rewritten as

$$\mathbf{Y} = \mathbf{S} + \underbrace{(\mathbf{HX} - \mathbf{S})}_{\text{MUI}} + \mathbf{W}, \tag{2}$$

For each user, the entry of $\mathbf{S}$ is assumed to be drawn from the same constellation. The second term in (2) represents the MUI signals. The total MUI energy can be measured as

$$P_{\text{MUI}} = \|\mathbf{HX} - \mathbf{S}\|_F^2. \tag{3}$$

It has been proven in [11] that the sum-rate of the downlink users can be maximized by minimizing the MUI energy in (3).

To guarantee the radar performance, we use a constant-modulus signal as the referenced waveform, and enforce a similarity constraint between the designed waveform and its referenced counterpart. Following [10], we employ the infinity norm in the constraint, and formulate the following optimization problem to minimize the MUI:

$$\min_{\mathbf{X}} \|\mathbf{HX} - \mathbf{S}\|_F^2 \tag{4a}$$

$$s.t \ \ \|\text{vec}(\mathbf{X} - \mathbf{X}_0)\|_\infty \le \eta, \ \ |x_{i,j}| = \sqrt{P_T/N}, \forall i, j, \tag{4b}$$

where $\mathbf{X}_0$ is the referenced radar signal, η is the tolerance threshold that ensures the similarity between the two waveforms, P_T denotes the total transmit power and $x_{i,j}$ is the (i, j)-th entry of $\mathbf{X}$. Note that both the objective function and the constraints in problem (4) are separable. Hence, it can be simplified using the normalized variables as

$$\begin{aligned} &\min_{\mathbf{x}} \left\| \sqrt{P_T/N}\mathbf{Hx} - \mathbf{s} \right\|^2 \\ &s.t \ \ \|\mathbf{x} - \mathbf{x}_0\|_\infty \le \varepsilon, \ \ |x(n)| = 1, \forall n, \end{aligned} \tag{5}$$

where $\varepsilon = \eta\sqrt{\frac{N}{P_T}}$, $\mathbf{x} \in \mathbb{C}^{N\times 1}$, $\mathbf{x}_0 \in \mathbb{C}^{N\times 1}$ are the columns of $\mathbf{X}$ and $\mathbf{X}_0$ normalized by $\sqrt{\frac{P_T}{N}}$, $\mathbf{s} \in \mathbb{C}^{K\times 1}$ is the column of $\mathbf{S}$, and $x(n)$ denotes the n-th entry of $\mathbf{x}$. Since problem (4) can be solved by solving the problem (5) for each column of $\mathbf{X}$ concurrently, we will focus on (5) in the following discussion. For notational convenience, we omit the column index.

Note that $0 \le \varepsilon \le 2$ since both $\mathbf{x}$ and $\mathbf{x}_0$ have unit modulus. The similarity constraint can be rewritten as [8]

$$\arg x(n) \in [l_n, u_n], \forall n, \tag{6}$$

where

$$\begin{aligned} l_n &= \arg x_0(n) - \arccos\left(1 - \varepsilon^2/2\right), \\ u_n &= \arg x_0(n) + \arccos\left(1 - \varepsilon^2/2\right), \end{aligned} \tag{7}$$

which leads to the following equivalent formulation of the problem

$$\begin{aligned} &\min_{\mathbf{x}} f(\mathbf{x}) = \left\| \tilde{\mathbf{H}}\mathbf{x} - \mathbf{s} \right\|^2 \\ &s.t. \ \ \arg x(n) \in [l_n, u_n], |x(n)| = 1, \forall n, \end{aligned} \tag{8}$$

where $\tilde{\mathbf{H}} = \sqrt{\frac{P_T}{N}}\mathbf{H}$. For each $x(n)$, the feasible region is an arc on the unit circle as shown in Fig. 1, which makes the problem non-convex, and NP-hard in general. In the following, we consider a global optimization algorithm for solving (8), which is based on the general framework of the branch-and-bound (BnB) methodology [12].

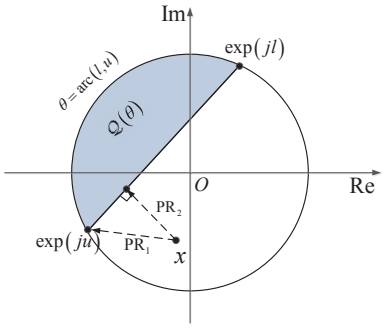

Fig. 1. Feasible region and convex hull of problem (8).

III. The Branch-and-bound Framework

A typical BnB algorithm requires to partition the feasible region into several subregions, where we formulate corresponding subproblems. For each subproblem, we obtain a sequence of asymptotic lower-bounds and upper-bounds by well-designed bounding functions. In each iteration, we update the bounds and the set of the subproblems following the BnB rules until convergence, i.e., the difference between the upper-bound and lower-bound goes to zero.

It is well understood that the worst-case complexity for the BnB algorithm is of exponential order with respect to N, i.e., corresponding to searching all branches of the subproblems exhaustively [12]. Nevertheless, by carefully choosing the tightest bounds, it is possible to efficiently identify and prune the unqualified branches, which accelerates the algorithm significantly.

Let us denote the feasible region, i.e., the arc shown in Fig. 1, as $\theta_n = \arc(l_n, u_n)$. Problem (8) can be compactly written as

$$\mathcal{P}(\Theta_0): \ \min_{\mathbf{x}} f(\mathbf{x}) \ \ s.t. \ \ \mathbf{x} \in \Theta_0. \tag{9}$$

where $\Theta_0 = \theta_1 \times \theta_2 \times ... \times \theta_N$, and $f(\mathbf{x})$ is defined in (8). By the above notations, a subproblem can be denoted as $\mathcal{P}(\Theta)$, where $\Theta \subseteq \Theta_0$ is the corresponding subregion. We then find the lower and upper bounds of $\mathcal{P}(\Theta)$ by the following bounding functions

$$f_L(\Theta) = f(\mathbf{x}_l), f_U(\Theta) = f(\mathbf{x}_u), \tag{10}$$

where $\mathbf{x}_l$ is a relaxed solution that achieves the lower-bound, and $\mathbf{x}_u$ is a feasible solution for $\mathcal{P}(\Theta)$ that yields the upper-bound. The above bounding functions will be specified in the next section. Here we only use f_L and f_U to introduce the BnB framework for notational convenience. In the BnB algorithm, we store all the subproblems in a problem set $\mathcal{S}$, which will be updated together with the global bounds in each iteration by the following rules [12]:

1) **Branching**: Pick a problem $\mathcal{P}(\Theta) \in \mathcal{S}$ that yields the smallest lower-bound. Equally divide Θ into two subregions following some subdivision rules detailed in the following, and generate two subproblems. Then delete $\mathcal{P}(\Theta)$ in the problem set.
2) **Pruning** (optional): Evaluate the qualification of the two subproblems, if their lower-bounds are less than the current global upper-bound, add them into $\mathcal{S}$.
3) **Bounding**: Choose the smallest lower-bound and upper-bound from $\mathcal{S}$ as the bounds for the next iteration.

Note that the pruning step is only for saving the memory of storing $\mathcal{S}$, and will not affect the effectiveness of the BnB procedure. This is because by choosing the smallest bounds in $\mathcal{S}$, one can always avoid the unqualified branches. For clarity, we summarize our BnB algorithm in Algorithm 1.

Algorithm 1 Branch-and-Bound Method for Solving (5)

Input: $\tilde{\mathbf{H}}, \mathbf{S}, \mathbf{x}_0$, $0 \leq \varepsilon \leq 2$, tolerance threshold $\delta > 0$, bounding functions f_L and f_U.

Initialization: Let Θ_0 be the initial feasible region of problem (27), $\mathcal{S} = \{\mathcal{P}(\Theta_0), f_U(\Theta_0), f_L(\Theta_0)\}$ be the initialized subproblem set. Set $UB = f_U(\Theta_0)$, $LB = f_L(\Theta_0)$.

while $UB - LB > \delta$ **do**

Branching

a) Pick $\mathcal{P}(\Theta) \in \mathcal{S}$, such that $f_L(\Theta) = LB$. Update $\mathcal{S} = \mathcal{S} \backslash \mathcal{P}(\Theta)$.

b) Divide Θ into Θ_A and Θ_B following the chosen subdivision rule.

Bounding

a) Compute $f_U(\Theta_i)$ and $f_L(\Theta_i)$ for $\mathcal{P}(\Theta_i), i = A, B$, and add them to $\mathcal{S}$.

b) Update UB and LB as the smallest upper-bound and lower-bound in $\mathcal{S}$, respectively.

end while

Output: $\mathbf{x}_{opt}$ = the feasible solution that achieves UB.

To ensure that Algorithm 1 converges in a finite number of iterations, the chosen subproblem for branching, the subdivision rule and the bounding functions f_L and f_U should satisfy the following conditions [12]:

1) The branching is bounding-improving, i.e., in each iteration we choose the problem that yields the smallest lower-bound as the branching node.
2) The subdivision is exhaustive, i.e., the maximum length of the subregions converges to zero as the iteration number goes to infinity.
3) The bounding is consistent with branching, i.e., $UB - f_{opt}$ converges to zero as the maximum length of the subregions goes to zero, where f_{opt} is the optimal value of the original problem.

Our Algorithm 1 satisfies condition 1) automatically. We then choose the subdivision rules to obtain the subproblems from the branching node. For a given node $\mathcal{P}(\Theta)$, we consider the following two rules:

- **Basic rectangular subdivision** (BRS): Equally divide Θ along $arc(l_n, u_n)$ and keep $arc(l_i, u_i), \forall i \neq n$ unchanged, where

$$n = \arg\max_n \{\phi_n | \phi_n = u_n - l_n\}. \tag{11}$$

- **Adaptive rectangular subdivision** (ARS): Equally divide Θ along $arc(l_n, u_n)$ and keep $arc(l_i, u_i), \forall i \neq n$ unchanged, where

$$n = \arg\max_n \{d_n | d_n = |x_u(n) - x_l(n)|\}. \tag{12}$$

In (12) $\mathbf{x}_u$ and $\mathbf{x}_l$ are the solutions associated with $f_U(\Theta)$ and $f_L(\Theta)$, respectively.

According to [12, Theorem 6.3 and 6.4], both the above two rules satisfy condition 2). In practical simulations, we observe that ARS has a faster convergence rate than BRS.

IV. Upper-bound and Lower-bound Acquisition

It remains to develop approaches to acquire the lower and upper bounds, which are key to accelerating the BnB procedure. Following the approach in [13], we compute the lower-bound by the convex relaxation of (9). As shown in Fig. 1, the convex hull for each entry $x(n)$, denoted as $\mathcal{Q}(\theta_n)$, is a circular segment, and can be given as

$$\mathcal{Q}(\theta_n) : \{x | \arg(x) \in \theta_n, |x| \leq 1\}. \tag{13}$$

By simple analytic geometry, the angle constraint can be equivalently written as

$$\mathrm{Re}\left(x^* \left(\frac{e^{ju} + e^{jl}}{2}\right)\right) \geq \cos\left(\frac{u-l}{2}\right), \tag{14}$$

which is nothing but a linear constraint. Hence the constraint for the vector variable is

$$\mathrm{Re}\left(\mathbf{x}^* \circ \left(\frac{e^{j\mathbf{u}} + e^{j\mathbf{l}}}{2}\right)\right) \geq \cos\left(\frac{\mathbf{u}-\mathbf{l}}{2}\right), \tag{15}$$

where $\mathbf{u} = [u_1, u_2, ..., u_N]^T \in \mathbb{R}^{N\times 1}, \mathbf{l} = [l_1, l_2, ..., l_N]^T \in \mathbb{R}^{N\times 1}$, and $\circ$ denotes the Hadamard product. The convex relaxation can be given as the following QCQP problem

$$\min_{\mathbf{x}} \left\|\tilde{\mathbf{H}}\mathbf{x} - \mathbf{s}\right\|^2 \tag{QP-LB}$$

$$s.t. \ \mathrm{Re}\left(\mathbf{x}^* \circ \left(\frac{e^{j\mathbf{u}} + e^{j\mathbf{l}}}{2}\right)\right) \geq \cos\left(\frac{\mathbf{u}-\mathbf{l}}{2}\right), |x(n)|^2 \leq 1, \tag{16}$$

Problem (16) can be efficiently solved via numerical solvers, e.g., the CVX toolbox. By doing so, we can readily obtain the lower-bound for each subproblem.

A natural way to compute the upper-bound is to project each entry of the obtained solution $\mathbf{x}_l$ of (16) on the corresponding arc to get a feasible solution. Such a projector can be shown intuitively in Fig. 1 as PR_1, where

$$\mathrm{PR}_1(x) = \arg\min_{\hat{x}} \|\hat{x} - x\|, \hat{x} \in \theta. \tag{17}$$

The upper-bound obtained by the projector (17) is still loose in general. To get a tighter bound, one can use $\mathrm{PR}_1(\mathbf{x}_l)$ as the initial point, and solve the following non-convex QCQP

$$\min_{\mathbf{x}} \left\| \tilde{\mathbf{H}}\mathbf{x} - \mathbf{s} \right\|^2 \tag{QP-UB}$$

$$s.t. \operatorname{Re}\left(\mathbf{x}^* \circ \left(\frac{e^{j\mathbf{u}} + e^{j\mathbf{l}}}{2}\right)\right) \geq \cos\left(\frac{\mathbf{u}-\mathbf{l}}{2}\right), |x(n)|^2 = 1, \tag{18}$$

which can be locally solved via the MATLAB *fmincon* solver that employs descent methods. Therefore, the obtained solution is guaranteed to yield a smaller value than $f(\mathrm{PR}_1(\mathbf{x}_l))$.

To further accelerate the speed for solving QP-LB and obtaining the bounds, we consider accelerated gradient projection (GP) methods [14] in addition to the QCQP solvers. Given $x_n \in \mathbb{C}$, the projector PR_2 projects x_n to the nearest point in the corresponding convex hull $\mathcal{Q}(\theta_n)$. Similarly, the projector PR_2 can be given in an element-wise manner as

$$\mathrm{PR}_2(x) = \arg\min_{\hat{x}} \|\hat{x} - x\|, \hat{x} \in \mathcal{Q}(\theta). \tag{19}$$

It should be noted that both PR_1 and PR_2 can be trivially obtained in closed-form by use of basic analytic geometry. Given the limited space, we will not show the detailed derivation in this paper.

Based on [14], our iterative scheme can be given in the form

$$\mathbf{v} = \mathbf{x}^{(k)} + \frac{k-1}{k+2}\left(\mathbf{x}^{(k)} - \mathbf{x}^{(k-1)}\right), \tag{20}$$

$$\mathbf{x}^{(k+1)} = \mathrm{PR}_2\left(\mathbf{v} - 2t\tilde{\mathbf{H}}^H\left(\tilde{\mathbf{H}}\mathbf{v} - \mathbf{s}\right)\right), \tag{21}$$

where we start from $\mathbf{x}^{(0)}$ and $\mathbf{x}^{(1)} = \mathbf{x}^{(0)}$. For the least-squares objective function, we choose the stepsize as $t = 1/\tilde{\lambda}_{\max}$, where $\tilde{\lambda}_{\max}$ is the maximum eigenvalue of $\tilde{\mathbf{H}}^H\tilde{\mathbf{H}}$, i.e., the Lipschitz constant. Note that the above iteration scheme can only be used for convex feasible regions due to the interpolation operation (20). For the non-convex QP-UB problem (18), we use $\mathbf{x}^{(k)}$ instead of the interpolated point $\mathbf{v}$, and replace the projector PR_2 with PR_1, which projects the point onto the arc, i.e., the feasible region. Similar to (16), we use $\mathrm{PR}_1(\mathbf{x}_l)$ as the initial point.

Remark 1: Based on [15], the complexity for using interior-point method to solve the QCQP problems is $\mathcal{O}(N^3)$ per iteration. For the proposed gradient-based methods, the costs are $\mathcal{O}(NK)$ in each iteration, which are far more efficient in terms of a fixed iteration number.

Remark 2: Since the proposed Algorithm 1 satisfies both conditions 1) and 2), the convergence of the algorithm can be proven by verifying that condition 3) holds. The proof is to simply apply the Lagrange Mean-Value Theorem to the Least-Squares objective function. Since the norm of the gradient of $f(x)$ is bounded by the Lipschitz constant $\tilde{\lambda}_{\max}$, it can be shown that the difference between the upper and lower bounds is also tightly upper-bounded. Finally, it can be trivially shown that this difference converges to zero as $\phi_{\max}$ or $d_{\max}$ goes to zero, where $\phi_{\max} = \max\{\phi_n\}, d_{\max} = \max\{d_n\}$, and ϕ_n and d_n are defined in (11) and (12).

Remark 3: While the worst-case complexity for the BnB approach is at the exponential order of N, our numerical results show that the proposed Algorithm 1 converges within only tens to hundreds iterations thanks to the well-designed bounding functions.

V. Numerical Results

In this section, we show the numerical results for solving the waveform optimization problem with constant modulus and similarity constraints. Following the simulation configurations in [10], we employ the orthogonal chirp waveform matrix as the reference signal. For convenience, we set $P_T = 1$, and each entry of the channel matrix $\mathbf{H}$ subject to standard Complex Gaussian distribution, i.e., $h_{i,j} \sim \mathcal{CN}(0,1)$. In all the simulations, we set $N = 16$ and employ a ULA with half-wavelength spacing between the adjacent antennas. The constellation chosen for the communication users is the unit-power QPSK alphabet.

The convergence behavior of the proposed BnB algorithm for solving (5) is shown in Fig. 2, with $N = 16, K = 4, \varepsilon = 1$, where we compare the performance of the two different subdivision rules, i.e., ARS and BRS. Both methods converge in a finite number of iterations with a nearly constant upper-bound, which suggests that one can reach the optimal value of problem (5) by iteratively using the local algorithms for several times, e.g., QCQP solver or the proposed gradient projection method. Nevertheless, due to the non-convexity of the problem, we need the BnB algorithm to confirm that this is indeed a global optimum. It can be also observed that the BnB-ARS has a faster convergence rate than BnB-BRS, which is consistent with the analysis in [12].

In Fig. 3 and 4, we show the trade-off between communication sum-rate and radar waveform similarity for the constant modulus designs, where the achievable sum-rate is computed based on [11, eq. (30)], and the SQR-Bisection Search (SQR-BS) algorithm is employed as our benchmark technique [10]. Fig. 3 demonstrates the communication sum-rate with increasing ε for $N = 16, K = 4, \mathrm{SNR} = 10\mathrm{dB}$. As expected, the proposed BnB algorithm outperforms the SQR-BS significantly, since the result obtained by BnB is the global optimum, while SQR-BS can only yields local minimum solutions. It is worth highlighting that the performance of BnB is very close to the convex relaxation bound, which is obtained by solving QP-LB. When the similarity tolerance ε is big enough, our BnB algorithm can fully eliminate the MUI.

Fig. 4 shows the results of radar pulse compression with different similarity tolerance ε, where we use the waveform

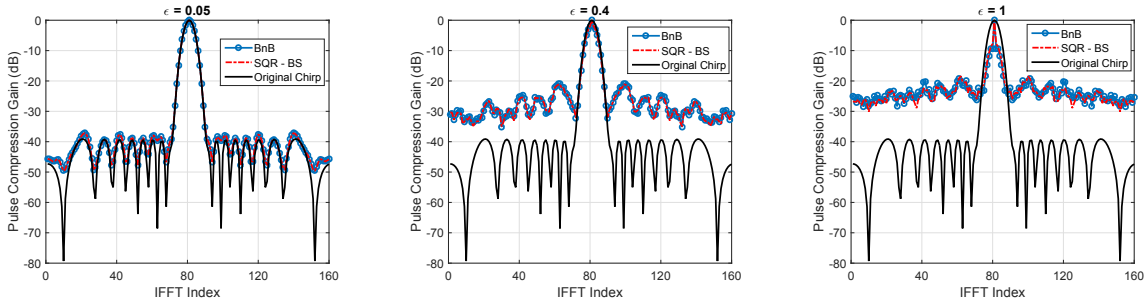

(a) (b) (c)

Fig. 4. Radar pulse compression for different similarity tolerance, $N = 16, K = 4$. (a) $\varepsilon = 0.05$; (b) $\varepsilon = 0.4$; (c) $\varepsilon = 1$.

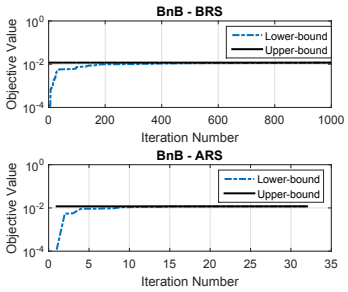

Fig. 2. Convergence Behavior of BnB Algorithm for $N = 16, K = 4, \varepsilon = 1$.

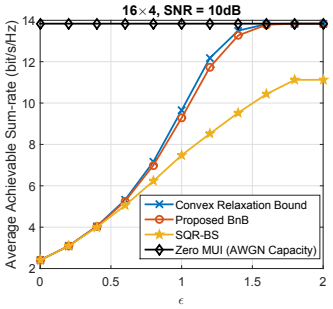

Fig. 3. Trade-off between the communication sum-rate and radar waveform similarity, $N = 16, K = 4, \text{SNR} = 10\text{dB}$.

transmitted by the first antenna, and employ the classical FFT-IFFT pulse compression method [16] with a Taylor window to reduce the sidelobes. Clearly, there exists a trade-off between the communication sum-rate and radar pulse compression performance. Moreover, the results for BnB and SQR-BS are nearly the same, as their performance is guaranteed by the same similarity constraint, which again proves the superiority of the proposed BnB Algorithm.

VI. Conclusion

This paper considers the constant-modulus waveform design for the dual-functional RadCom system, where we minimize the multi-user interference under both constant-modulus and radar signal similarity constraints. While the optimization problem is non-convex, and NP-hard in general, it can be efficiently solved via a well-designed branch-and-bound (BnB) algorithm. Numerical results show that the proposed approach significantly outperforms the conventional SQR-BS algorithm by obtaining the global minimizer of the problem.

References

[1] DARPA. (2016) Shared spectrum access for radar and communications (SSPARC). [Online]. Available: http://www.darpa.mil/program/shared-spectrum-access-for-radar-and-communications

[2] B. Li and A. Petropulu, "Joint transmit designs for co-existence of MIMO wireless communications and sparse sensing radars in clutter," *IEEE Trans. Aerosp. Electron. Syst.*, vol. 53, no. 6, pp. 2846–2864, Dec 2017.

[3] F. Liu, C. Masouros, A. Li, and T. Ratnarajah, "Robust MIMO beamforming for cellular and radar coexistence," *IEEE Wireless Commun. Lett.*, vol. 6, no. 3, pp. 374–377, June 2017.

[4] L. Zheng, M. Lops, X. Wang, and E. Grossi, "Joint design of overlaid communication systems and pulsed radars," *IEEE Trans. Signal Process.*, vol. 66, no. 1, pp. 139–154, Jan 2018.

[5] A. Hassanien, M. G. Amin, Y. D. Zhang, and F. Ahmad, "Dual-function radar-communications: Information embedding using sidelobe control and waveform diversity," *IEEE Trans. Signal Process.*, vol. 64, no. 8, pp. 2168–2181, April 2016.

[6] ——, "Phase-modulation based dual-function radar-communications," *IET Radar Sonar Nav.*, vol. 10, no. 8, pp. 1411–1421, 2016.

[7] F. Liu, C. Masouros, A. Li, H. Sun, and L. Hanzo, "MU-MIMO communications with MIMO radar: From co-existence to joint transmission," *IEEE Trans. Wireless Commun.*, vol. PP, no. 99, pp. 1–1, 2018.

[8] G. Cui, H. Li, and M. Rangaswamy, "MIMO radar waveform design with constant modulus and similarity constraints," *IEEE Trans. Signal Process.*, vol. 62, no. 2, pp. 343–353, Jan 2014.

[9] F. Liu, C. Masouros, P. V. Amadori, and H. Sun, "An efficient manifold algorithm for constructive interference based constant envelope precoding," *IEEE Signal Process. Lett.*, vol. 24, no. 10, pp. 1542–1546, Oct 2017.

[10] O. Aldayel, V. Monga, and M. Rangaswamy, "Successive QCQP refinement for MIMO radar waveform design under practical constraints," *IEEE Trans. Signal Process.*, vol. 64, no. 14, pp. 3760–3774, July 2016.

[11] S. K. Mohammed and E. G. Larsson, "Per-antenna constant envelope precoding for large multi-user MIMO systems," *IEEE Trans. Commun.*, vol. 61, no. 3, pp. 1059–1071, March 2013.

[12] H. Tuy, *Convex Analysis and Global Optimization*. Springer International Publishing, 2016.

[13] C. Lu and Y. F. Liu, "An efficient global algorithm for single-group multicast beamforming," *IEEE Trans. Signal Process.*, vol. 65, no. 14, pp. 3761–3774, July 2017.

[14] Y. Nesterov, "Introductory lectures on convex optimization," *Applied Optimization*, vol. 87, no. 5, pp. xviii,236, 2004.

[15] M. S. Lobo, L. Vandenberghe, S. Boyd, and H. Lebret, "Applications of second-order cone programming," *Linear algebra and its applications*, vol. 284, no. 1-3, pp. 193–228, 1998.

[16] M. A. Richards, *Fundamentals of radar signal processing*. Tata McGraw-Hill Education, 2005.